Electronic Supplementary Materials

Solution-processable *n*-doped graphene-containing interfacial cathode materials for high performance organic solar cells

Fei Pan[‡,b,c], Chenkai Sun[‡,b,c], Yingfen Li[a], Dianyong Tang[d], Yingping Zou[e], Xiaojun Li[b,c], Song Bai[a], Xian Wei[a], Menglan Lv[*,a,b] , Xiwen Chen[f], Yongfang Li[*,b,c]

[a] School of Chemical Engineering, Guizhou Institute of Technology, Guiyang, Guizhou 550003, China.

[b] Beijing National Laboratory for Molecular Sciences, CAS Key Laboratory of Organic Solids, Institute of Chemistry, Chinese Academy of Sciences, Beijing 100190, China.

[c] School of Chemical Science, University of Chinese Academy of Sciences, Beijing 100049, China.

[d] Chongqing Engineering Laboratory of Targeted and Innovative Therapeutics, International Academy of Targeted Therapeutics and Innovation, Chongqing University of Arts and Sciences, Chongqing 402160, China.

[e] College of Chemistry and Chemical Engineering, Central South University, Changsha, Hunan 410083, China

[f] Guangzhou Polyforte Chemical Technology Co. LTD, Guangzhou, Guangdong 510520, China.

1. **Simulation Method.**

Periodic density functional theory calculations were carried out by SIESTA package[1,2] with Troullier–Martins norm conserving pseudopotentials.[3] The exchange–correlation functional utilized was at the generalized gradient approximation level, known as GGA-PBE. [2] The optimized double-z plus polarization basis set with extra diffuse function was employed for metal. The orbital-confining cutoff was determined from an energy shift of 0.010 eV. The energy cutoff for the real space grid used to represent the density was set as 150 Ry. The Grimme method was chosen for DFT-D correction [3]. Spin-polarized calculations were carried out. The Quasi-Newton l-BFGS method is used for geometry relaxation until the maximal force on each degree of freedom is less than 0.05 eV. $Å^{-1}$. The Γ-point was chosen in the Brillouin zone integration for a larger 10×10 supercell of graphene, which contains 200 carbon atoms. The slab supercell considered has been carefully tested, and a 35 Å vacuum along the c axis has been adopted to ensure no reciprocal interaction between periodic images. All the atoms of graphene were allowed to relax along with the adsorbates. The adsorption energies (E_{ad}) for all possible adsorbates were calculated according to

$$E_{ad} = E_{gas\text{-}graphene} - (E_{gas} + E_{graphene})$$

where $E_{gas\text{-}graphene}$, E_{gas}, and $E_{graphene}$ are total energies of the adsorbed species on graphene, the clean graphene surface, and the corresponding gas-phase species, respectively.

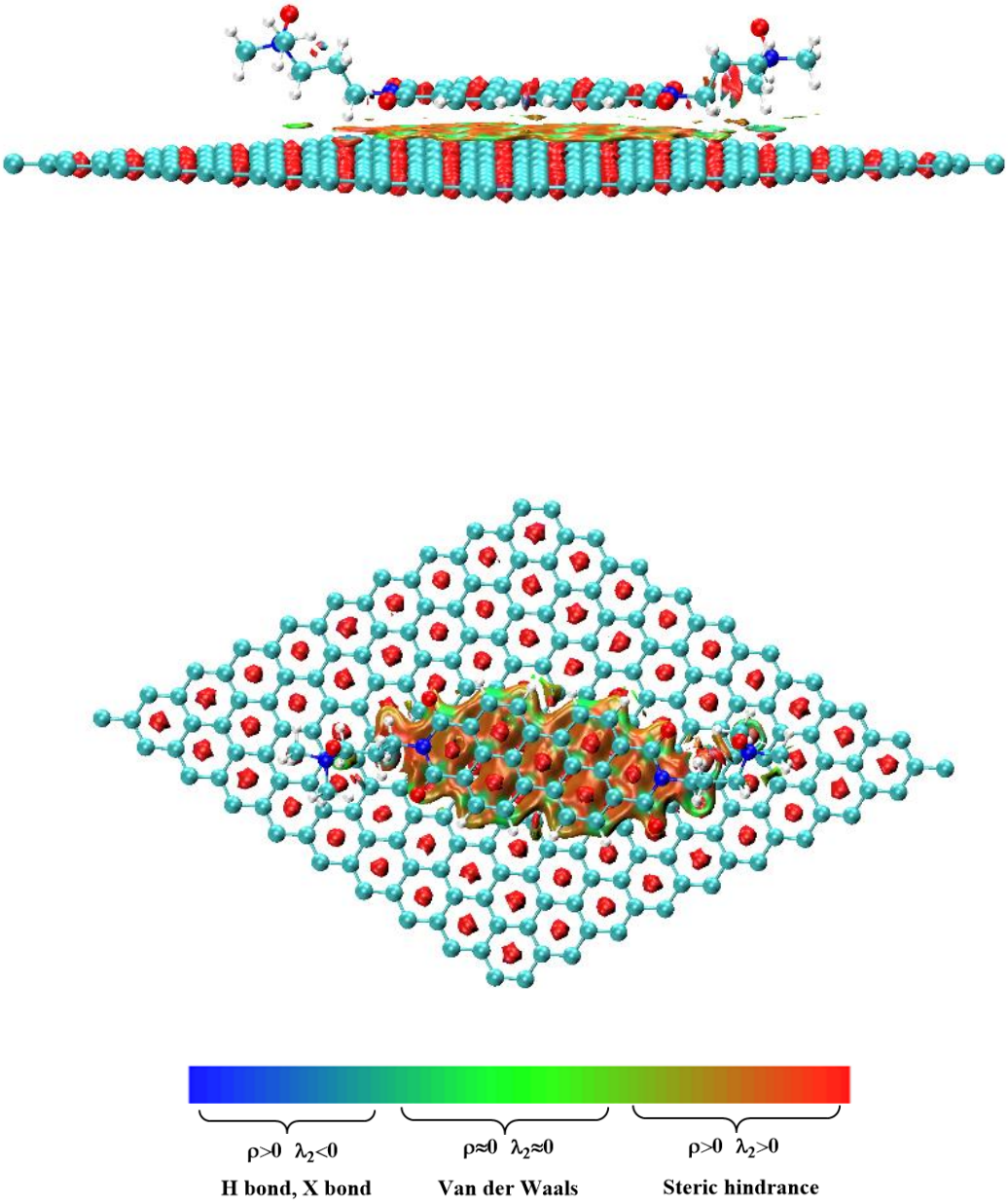

Fig. S1 Reduced density gradient isosurface plot for PDINO-graphene complex.

Table S1 Adsorption energies of different surfactants on the graphene surface estimated by periodic density functional theory calculations.

Chemical structure	Adsorption Energies on Graphene Surface (eV)

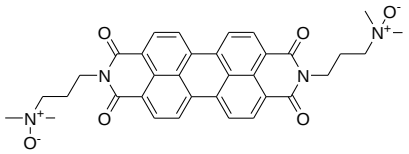 **PDINO**	-3.510
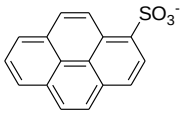 **PSA** 1-pyrenesulfonic acid sodium salt	-0.438
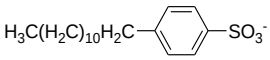 **SDBS** Sodium dodecylbenzenesulfonate	-0.271

2. Tyndall effect of graphene dispersion

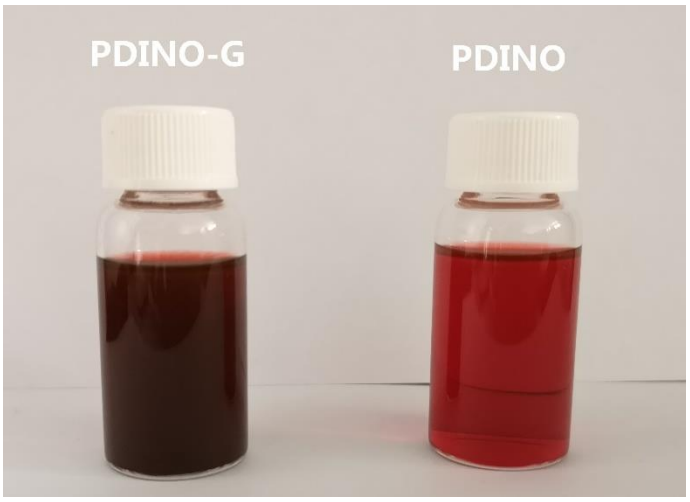

Fig. S2 Photograph of PDINO-G dispersion (2 mg mL^{-1} PDINO with 5% graphene) and PDINO solution (2 mg mL^{-1}).

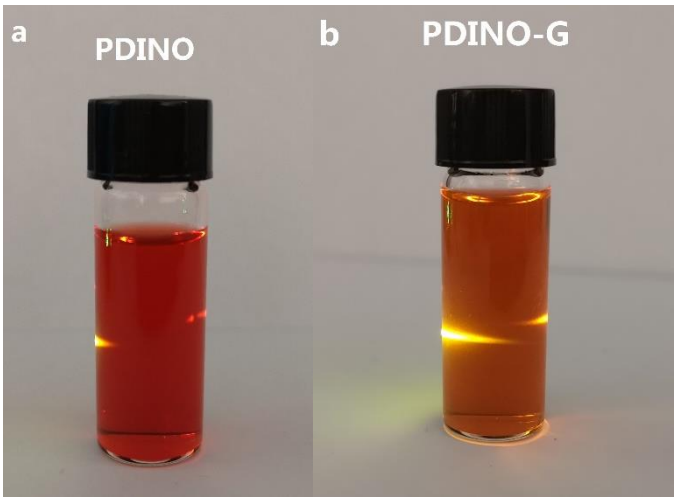

Fig. S3 Photograph of (a) PDINO solution (1 mg mL^{-1}), (b) Tyndall effect of a dispersion of the PDINO-G (1 mg mL^{-1} with 5% graphene).

3. X-ray diffraction measurement for PDINO dispersive graphene

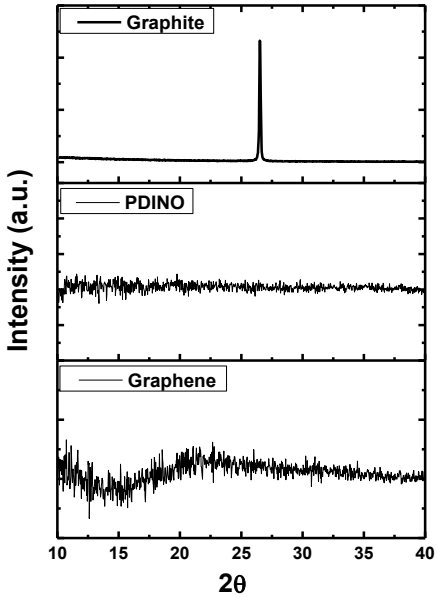

Fig. S4 XRD patterns for PDINO, graphite and dispersed graphene.

4. Laser Raman spectra for dispersive graphene

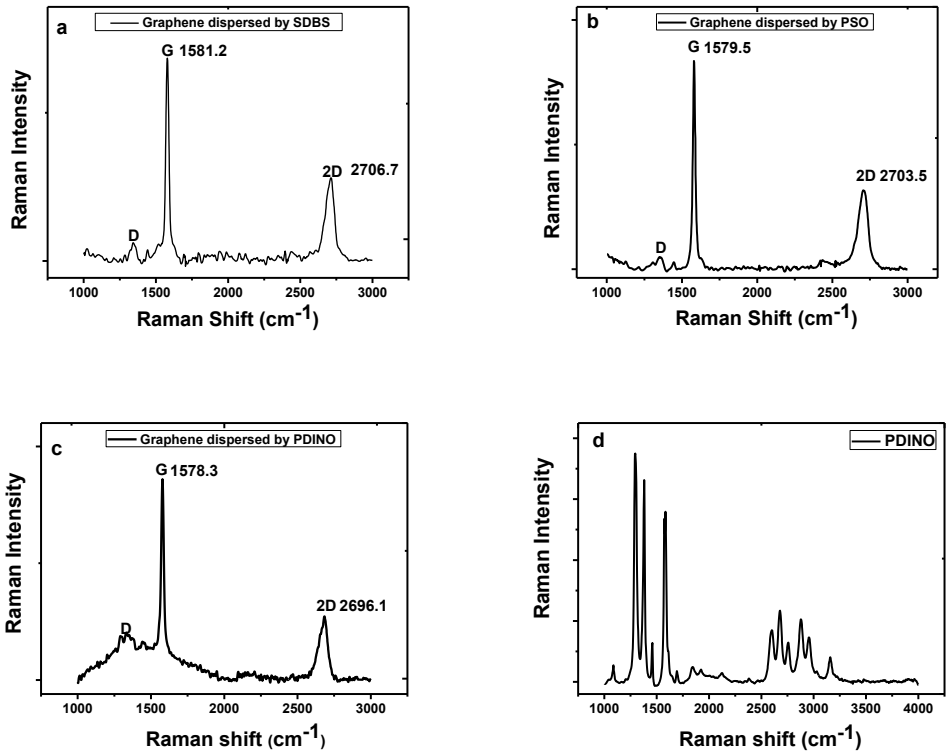

Fig. S5 Full Raman spectrum for (a) graphene dispersed with SDBS, (b) graphene dispersed with PSO, (c) graphene dispersed with PDINO, (d) pure PDINO.

5. X-ray photoelectron spectroscopy for graphene power

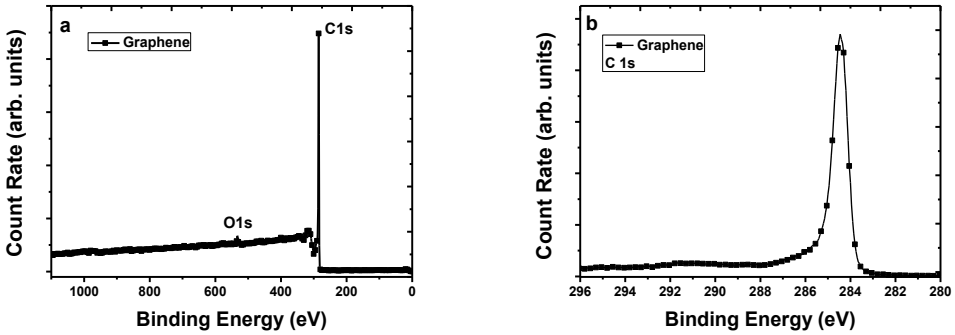

Fig. S6 XPS full spectrum (a) and C 1s (b) spectrum of graphene power.

6. Optimized doping ratio of interfacial modification

Table S2 The device performance of the OSCs based on PTQ10: IDIC-2F with different ration of graphene in PDINO-G interfacial modification under the illumination of AM 1.5 G, 100 mW cm^{-2}.

The ratio of graphene	V_{oc} [V]	J_{sc} [mA cm^{-2}]	*FF* [%]	*PCE* [%]
1%	0.90	17.82	71.66	11.49
2%	0.90	18.13	71.76	11.71
3%	0.90	18.43	72.25	11.98
4%	0.91	18.36	72.88	12.18
5%	0.91	18.54	73.52	12.40
6%	0.91	18.46	73.07	12.27
7%	0.90	18.53	72.07	12.02
8%	0.90	18.45	72.60	12.06
9%	0.90	18.12	72.60	11.84
10%	0.90	17.90	72.43	11.67
20%	0.90	17.92	71.60	11.51

Table S3 The device performance of the OSCs based on PTQ10: IDIC-2F with different ration of GO in PEDOT: PSS-GO interfacial modification under the illumination of AM 1.5 G, 100 mW cm^{-2}.

The ratio of GO	V_{oc} [V]	J_{sc} [mA cm^{-2}]	*FF* [%]	*PCE* [%]
0.1%	0.90	17.89	73.75	11.87
0.3%	0.90	18.08	73.90	12.06
0.5%	0.90	18.39	73.92	12.23
0.7%	0.90	18.30	73.22	12.03
0.9%	0.89	17.95	73.47	11.74
1.2%	0.89	17.88	72.17	11.48

Table S4 The device performance of the OSCs based on PTQ10: IDIC with different ration of graphene in PDINO-G interfacial modification under the illumination of AM 1.5 G, 100 mW cm^{-2}.

The ratio of graphene	V_{oc} [V]	J_{sc} [mA cm^{-2}]	*FF* [%]	*PCE* [%]
1%	0.96	17.06	71.90	11.78
2%	0.96	17.23	72.22	11.95
3%	0.96	17.29	72.51	12.03
4%	0.96	17.31	72.86	12.11
5%	0.96	17.08	72.79	11.94
6%	0.96	16.94	71.82	11.75
7%	0.96	16.85	71.58	11.58
8%	0.95	16.61	71.89	11.34
9%	0.95	16.49	72.13	11.29
10%	0.95	16.63	71.80	11.30
20%	0.94	16.77	71.05	11.20

Table S5 The device performance of the OSCs based on PTQ10: IDIC with different ration of GO in PEDOT: PSS-GO interfacial modification under the illumination of AM 1.5 G, 100 mW cm^{-2}.

The ratio of GO	V_{oc} [V]	J_{sc} [mA cm^{-2}]	*FF* [%]	*PCE* [%]
0.1%	0.96	17.11	72.86	11.94
0.3%	0.96	17.06	73.47	12.03
0.5%	0.96	16.87	73.53	11.90
0.7%	0.96	16.64	72.93	11.65
0.9%	0.96	16.41	72.94	11.49
1.2%	0.96	16.57	72.22	11.45

7. Scanning Kelvin Probe Microscopy measurement

Table S6 Work functions of PEDOT: PSS-GO on ITO substrates measured by Scanning Kelvin Probe Microscopy in air. The work function of ITO was set as 4.70 eV, and errors of measured work function are ±0.03eV.

Top layer / Substrate	None [eV]	PEDOT: PSS [eV]	0.1%GO/ PEDOT:PSS [eV]	0.5%GO/ PEDOT:PSS [eV]	1%GO/ PEDOT:PSS [eV]	2%GO/ PEDOT:PSS [eV]
ITO	4.70	5.11	5.06	5.00	4.98	4.94

8. Optical Properties.

Fig. S7 shows the absorption spectra of PDINO-G with different graphene ratio in ethanol solution and in thin films spun cast on quartz plates. In solution, the composite material PDINO-G shows similar absorption spectrum with PDINO because the dispersed PDINO molecules in the composite solution show similar situation with that in the pure PDINO solution. While in the solid state, aggregation could exist between PDINO molecules and between PDINO and graphenes, so that the solid film of the composites shows some difference in absorption spectra in comparison with their solutions. The graphene dispersed in PDINO could reduce the interaction among PDI rings. This could make the main absorption peak blue-shifted (see Fig S7b and Table S7). The PL intensity of the PDINO-G increased with the increase of the graphene content, as shown in Fig S7c, which indicates that the *n*-doping of PDINO into graphene enhanced the PL of PDINO.

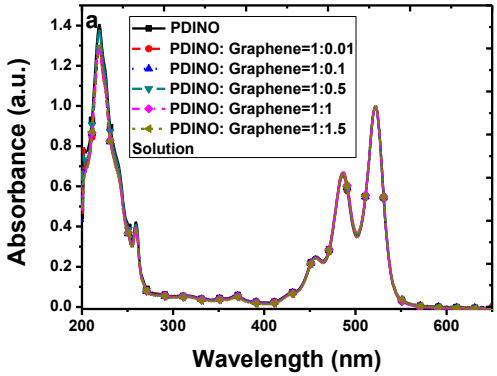

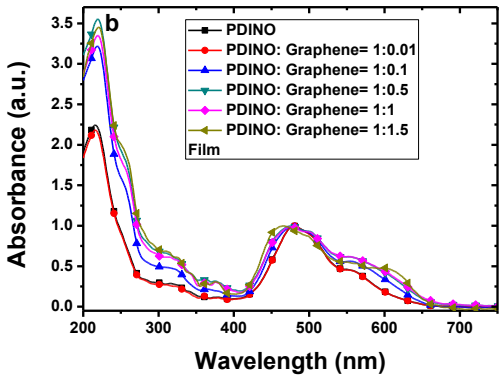

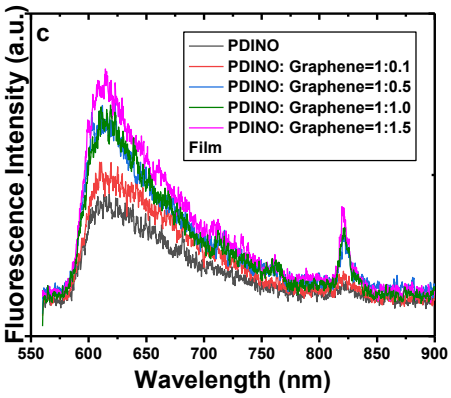

Fig. S7 Ultraviolet-visible absorption spectra of PDINO-G with different graphene ratio (a) ethanol solution, (b) thin films spun cast on quartz plates, (c) fluorescence spectra of pure PDINO and PDINO-G excited at 550 nm.

Table S7 The wavelength of maximum absorption peak during 400-700 nm from Ultraviolet-visible absorption spectra for PDINO-G with different graphene ratio.

The ratio of PDINO: Graphene	1:0	1:0.01	1:0.10	1:0.50	1:1.00	1:1.50
λ_{max}(nm)	480	479	476	476	474	466

9. Conductivity and HOMO of PDINO-G cathode interlayer measurement.

Two-point probe devices were fabricated using organic ribbon mask technique measurements. In order to minimize artificial effects such as contact resistance, all PDINO-G films spun for the electrical measurements were thick around 35 nm. All devices were measured in air at room temperature. Figure S6b showed the two-point probe J-V curves for the PDINO-G with different graphene ratio (without gate). The extracted conductance for PDINO and PDINO-G are in good agreement with those measured by the SCLC method.

Table S8 HOMO of PDINO-G with various ratio measured by UPS. Conductivity of PDINO-G with various ratio measured by SCLC model and two-point probe devices, respectively.

		PDINO	5%G /PDINO	10%G /PDINO	20%G /PDINO
HOMO [eV]		5.88	5.98	6.05	6.21
Conductivity [S cm^{-1}]	SCLC	9.14×10^{-6}	1.18×10^{-3}	2.67×10^{-3}	4.25×10^{-3}
	Two-Point	9.49×10^{-6}	7.29×10^{-4}	2.11×10^{-3}	8.21×10^{-3}

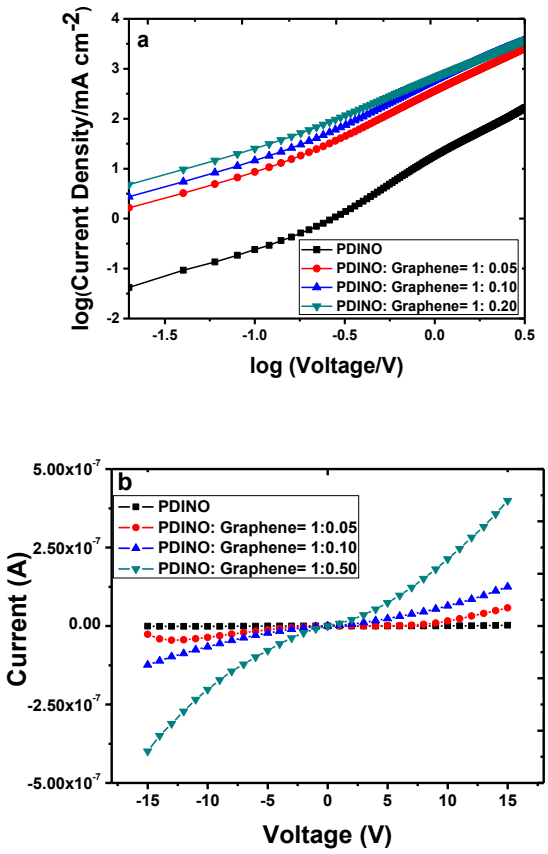

Fig. S8 (a) *J-V* characteristics from SCLC model of conductivity device, (b) two-terminal *J-V* characteristics (V_G=0 V) of two-point probe devices for conductance measurement of PDINO-G with different graphene ratio.

10. Electron spin resonance (ESR) spectroscopy

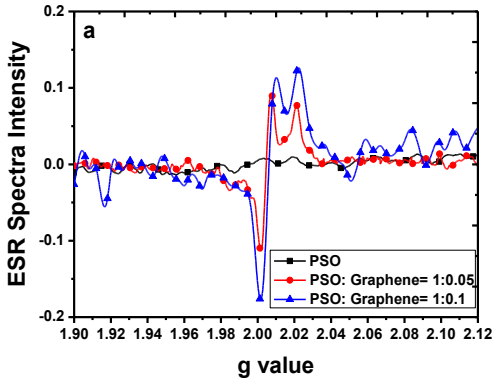

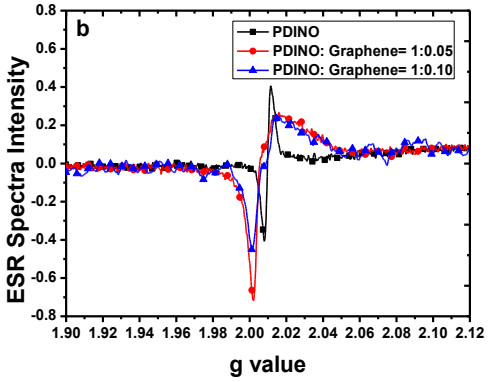

Fig. S9 ESR spectra of (a) PDINO and PDINO-G with different graphene ratio (b)PSO and PSO-G with different graphene ratio.

11. X-ray photoelectron spectroscopy (XPS) spectra

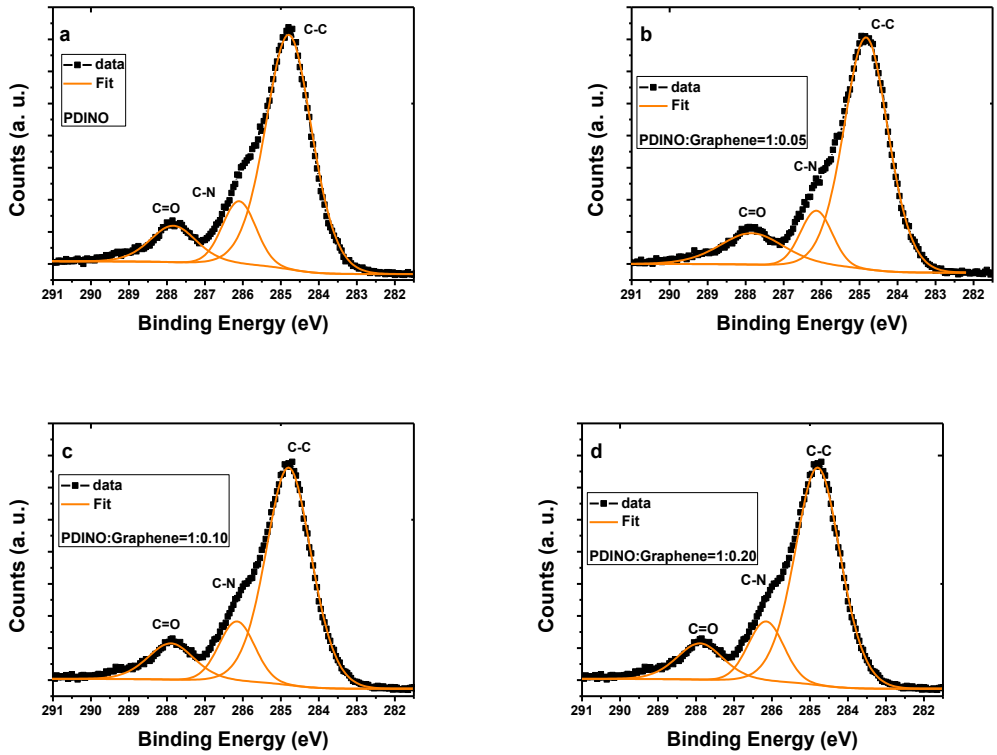

Fig. S10 XPS C 1s spectrum of (a) PDINO, (b) PDINO-G with 5% graphene, (c) PDINO-G with 10% graphene, (d) PDINO-G with 20% graphene.

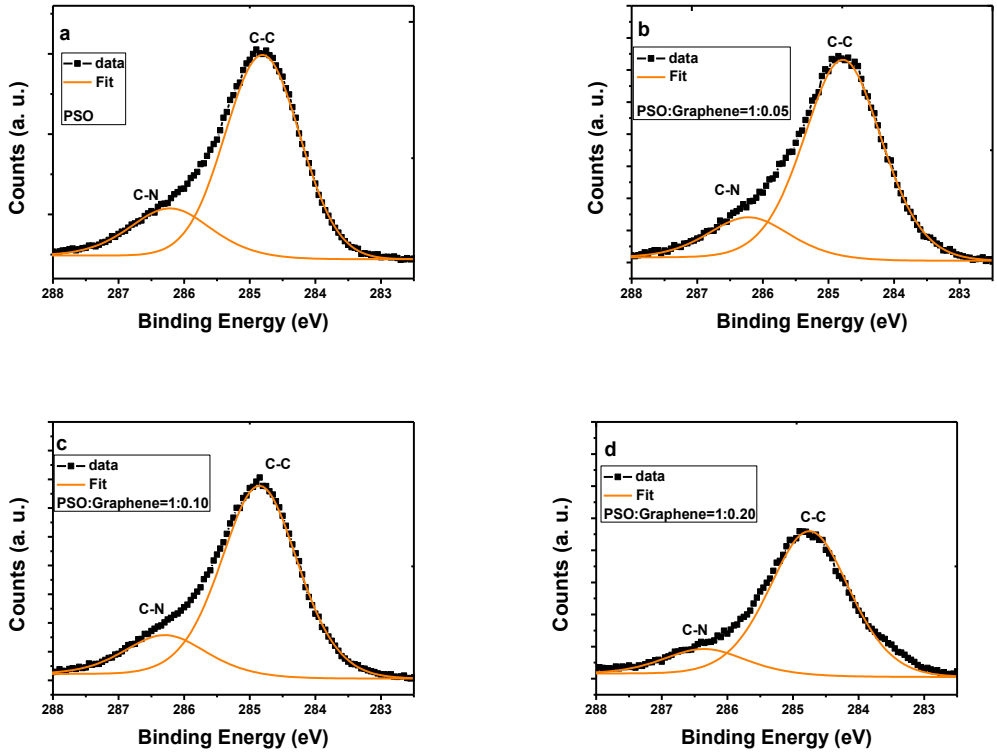

Fig. S11 XPS C 1s spectrum of (a) PSO, (b) PSO-G with 5% graphene, (c) PSO-G with 10%

graphene, (d) PSO-G with 20% graphene.

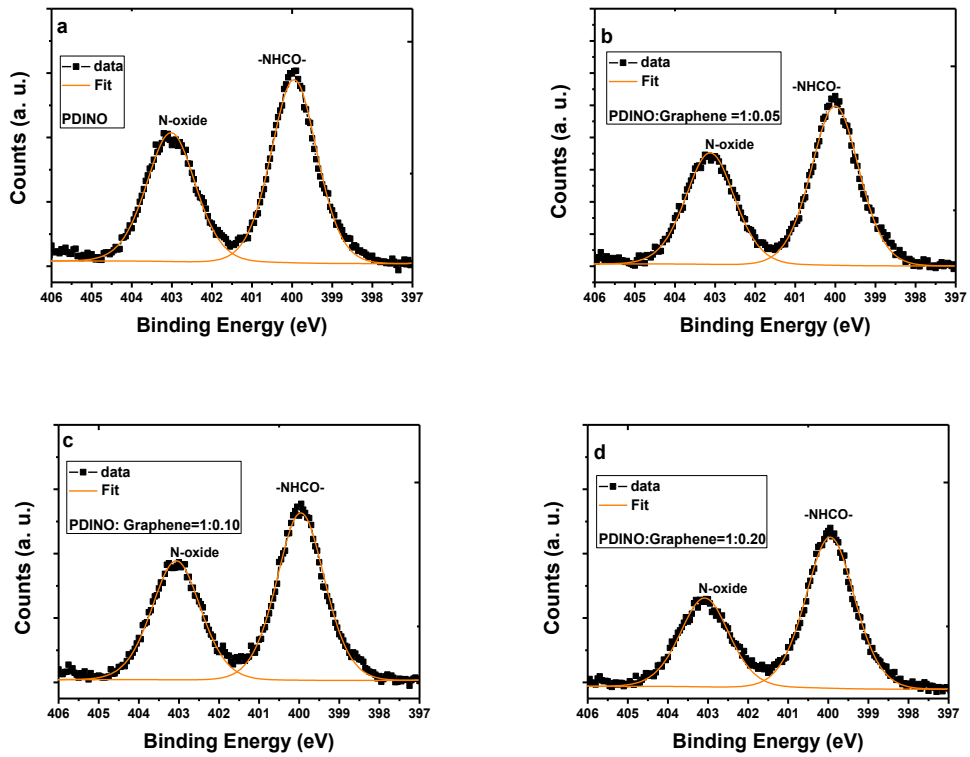

Fig. S12 XPS N 1s spectrum of (a) PDINO, (b) PDINO-G with 5% graphene, (c) PDINO-G with 10% graphene, (d) PDINO-G with 20% graphene.

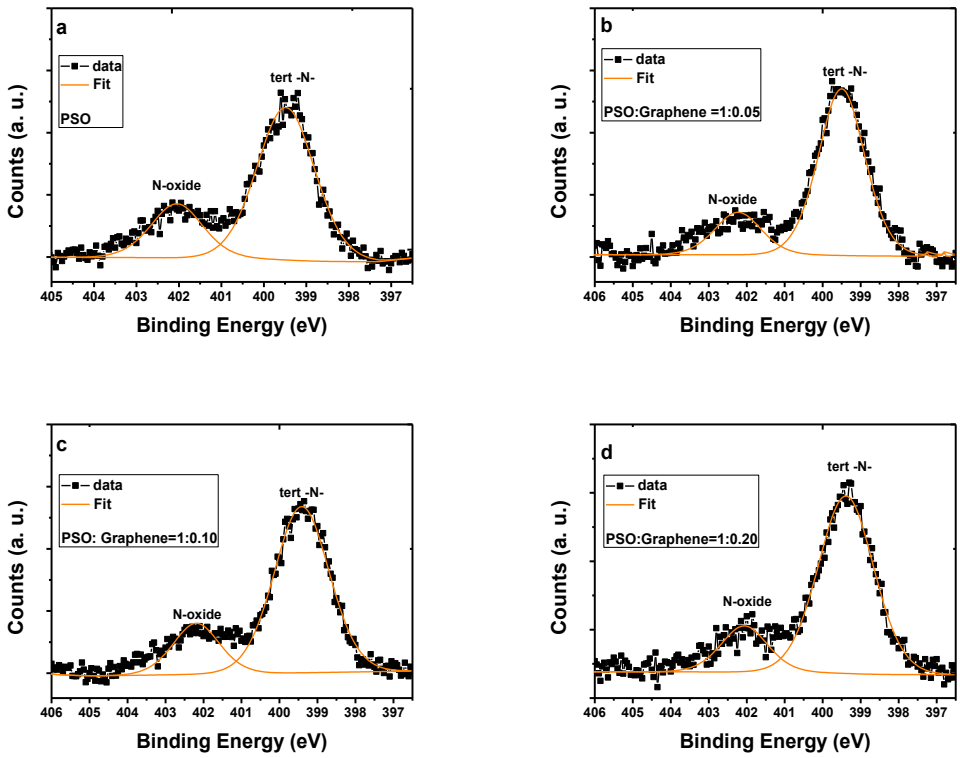

Fig. S13 XPS N 1s spectrum of (a) PSO, (b) PSO-G with 5% graphene, (c) PSO-G with 10%

graphene, (d) PSO-G with 20% graphene.

12. Fabrication of Electron-only and Hole-only Devices.

The mobility was determined by fitting the dark *J-V* curves to the model of a single-carrier SCLC model [4,] described as Equation: $J=9\varepsilon_r\varepsilon_0\mu V^2/8L^3$, where J is the current, μ is the zero-field mobility, ε_0 is the permittivity of free space, ε_r is the relative permittivity of the material, L is the thickness of the active layers. The hole-only device with the device structure of ITO/PEDOT: PSS or PEDOT: PSS-GO/PTQ10: IDIC-2F/with or without different cathode interlayer/MoO_3 (5 nm)/Au (50 nm) was used to measure the hole mobility, and the electron-only device with the device structure of ITO/ZnO (10 nm)/PTQ10: IDIC-2F/with or without different cathode interlayer/Al (100 nm) was used to measure the electron mobility.

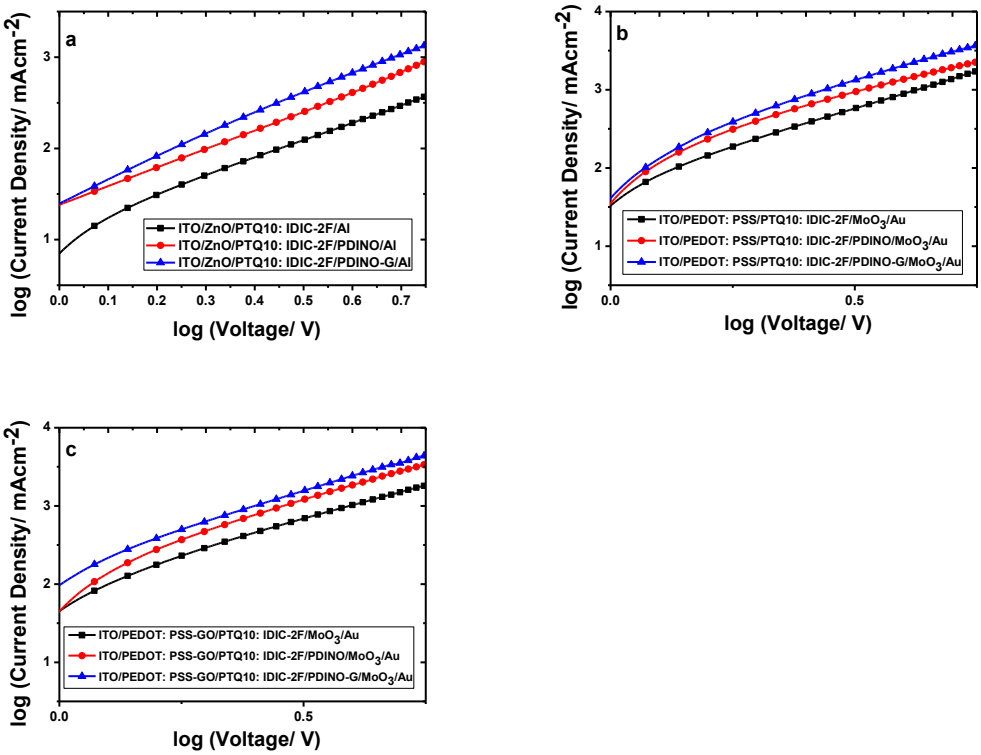

Fig. S14 *J-V* characteristics from SCLC model of (a) electron-only devices of OSCs ITO/ZnO/PTQ10: IDIC-2F/with or without different cathode interlayer/Al and hole-only devices of OSCs (b) ITO/PEDOT: PSS/PTQ10: IDIC-2F/with or without different cathode interlayer/MoO_3 (5 nm)/Au (50 nm) and (c) ITO/ PEDOT: PSS-GO/PTQ10: IDIC-2F/with or without different cathode interlayer/MoO_3 (5 nm)/Au (50 nm)

Table S9 Hole and electron mobilities of the devices with various interfacial treatment.

	Single-carrier Device Structure	Mobiliy (cm^2/Vs)
Hole-only devices	ITO/PEDOT: PSS/BHJ/MoO_3/Au	9.43×10^{-4}
	ITO/PEDOT: PSS/ BHJ/PDINO/MoO_3/Au	1.68×10^{-3}
	ITO/PEDOT: PSS/BHJ/PDINO-G/MoO_3/Au	3.14×10^{-3}
	ITO/PEDOT: PSS-GO/BHJ /MoO_3/Au	9.61×10^{-4}
	ITO/PEDOT: PSS-GO/BHJ/PDINO/MoO_3/Au	2.47×10^{-3}
	ITO/PEDOT: PSS-GO/BHJ/PDINO-G/MoO_3/Au	3.96×10^{-3}
Electron-only devices	ITO/ZnO/BHJ/Al	2.34×10^{-4}
	ITO/ZnO/BHJ/PDINO/Al	7.52×10^{-4}
	ITO/ZnO/BHJ/PDINO-G/Al	2.48×10^{-3}

13. Thickness sensitivity analysis

Table S10 Photovoltaic performance data of the OSCs based on PTQ10: IDIC-2F with different thickness of PDINO-G under the optimized conditions (ITO/PEDOT: PSS-GO/PTQ10: IDIC-2F/PDINO-G/Al)

The thickness of PDINO-G	V_{oc} [V]	J_{sc} [mA cm^{-2}]	*FF* [%]	PCE_{max} [%]	PCE_{avg} [%]
5 nm	0.91	19.09	74.87	13.01	12.8±0.2
10 nm	0.91	18.89	74.66	12.84	12.5±0.3
18 nm	0.91	18.83	74.18	12.71	12.4±0.3
32 nm	0.91	18.76	73.72	12.60	12.4±0.2

14. Generality for different BHJ systems

Table S11 Photovoltaic performance data of the OSCs based on PTQ10: IDIC-2F with different interfacial modification under the illumination of AM 1.5 G, 100 mW cm^{-2}.

Structure of OSCs with different interfacial modification	*Voc* [V]	*Jsc(Jcalc.*[a]*)* [mA cm^{-2}]	*FF* [%]	PCE_{max} [%]	PCE_{avg} [%]
ITO/PEDOT: PSS/ BHJ /Al	0.84	17.89(17.37)	67.55	10.15	9.9±0.3
ITO/PEDOT: PSS/BHJ/PDINO/Al	0.90	18.06(17.53)	72.66	11.81	11.5±0.3
ITO/ PEDOT:PSS-GO/BHJ/PDINO-G/Al	0.91	19.09(18.31)	74.87	13.01	12.8±0.2
ITO/ PEDOT:PSS-GO/BHJ/PDINO-G/Ag	0.90	18.91(18.34)	68.53	11.66	11.4±0.3
ITO/ PEDOT:PSS-GO/BHJ/PDINO-G/Au	0.89	17.01(16.50)	69.31	10.49	10.2±0.3

[a] The J_{calc} from the EQE spectrum

Table S12 Photovoltaic performance data of the OSCs based on PTQ10: IDIC with different interfacial modification under the illumination of AM 1.5 G, 100 mW cm^{-2}.

Structure of OSCs with different interfacial modification	*Voc* [V]	*Jsc(Jcalc.*[a]*)* [mA cm^{-2}]	*FF* [%]	PCE_{max} [%]	PCE_{avg} [%]
ITO/PEDOT: PSS/BHJ/Al	0.93	16.44(15.95)	66.06	10.10	9.8±0.3
ITO/PEDOT: PSS/BHJ/PDINO/Al	0.96	16.80(16.30)	72.02	11.56	11.3±0.3
ITO/PEDOT:PSS-GO /BHJ/PDINO-G/Al	0.96	17.43(16.91)	74.34	12.44	12.2±0.2
ITO/PEDOT:PSS-GO/BHJ/PDINO-G/Ag	0.95	17.55(17.02)	68.48	11.42	11.1±0.3
ITO/PEDOT:PSS-GO/BHJ/PDINO-G/Au	0.95	15.84(15.36)	68.51	10.31	9.7±0.3

[a] The J_{calc} from the EQE spectrum

Table S13 Photovoltaic performance data of the OSCs based on PM6:Y6 with different interfacial modification under the illumination of AM 1.5 G, 100 mW cm^{-2}.

Structure of OSCs with different interfacial modification	V_{oc} [V]	$J_{sc}(J_{calc.}$[a]$)$ [mA cm^{-2}]	*FF* [%]	PCE_{max} [%]	PCE_{avg} [%]
ITO/PEDOT: PSS/ BHJ/Al	0.82	24.15(23.67)	66.95	13.26	12.9±0.3
ITO/PEDOT: PSS/BHJ/PDINO/Al	0.84	24.84(24.34)	73.43	15.32	15.1±0.2
ITO/PEDOT:PSS-GO/BHJ/PDINO-G/Al	0.85	25.65(25.14)	75.78	16.52	16.3±0.2
ITO/PEDOT:PSS-GO/BHJ/PDINO-G/Ag	0.84	25.68(25.17)	68.81	14.84	14.5±0.3
ITO/PEDOT:PSS-GO/BHJ/PDINO-G/Au	0.83	24.05(23.57)	68.86	13.75	13.4±0.3

[a] The J_{calc} from the EQE spectrum

15. Film morphology for PDINO dispersive graphene

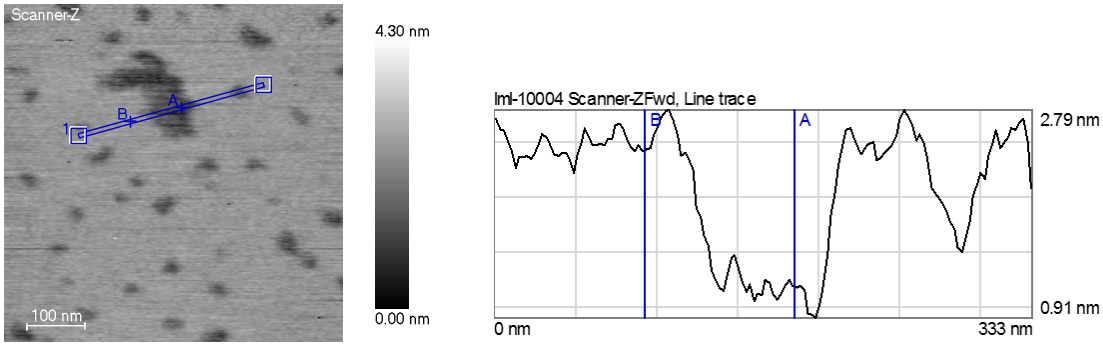

Fig. S15 AFM (3×3 μm) images of AFM image (top) of the few-layered graphene flakes deposited on a mica substrate. Bottom: Height profile corresponding to the line shown in the AFM image. (b) Thickness distribution of 50 graphene flakes in the inset AFM image.

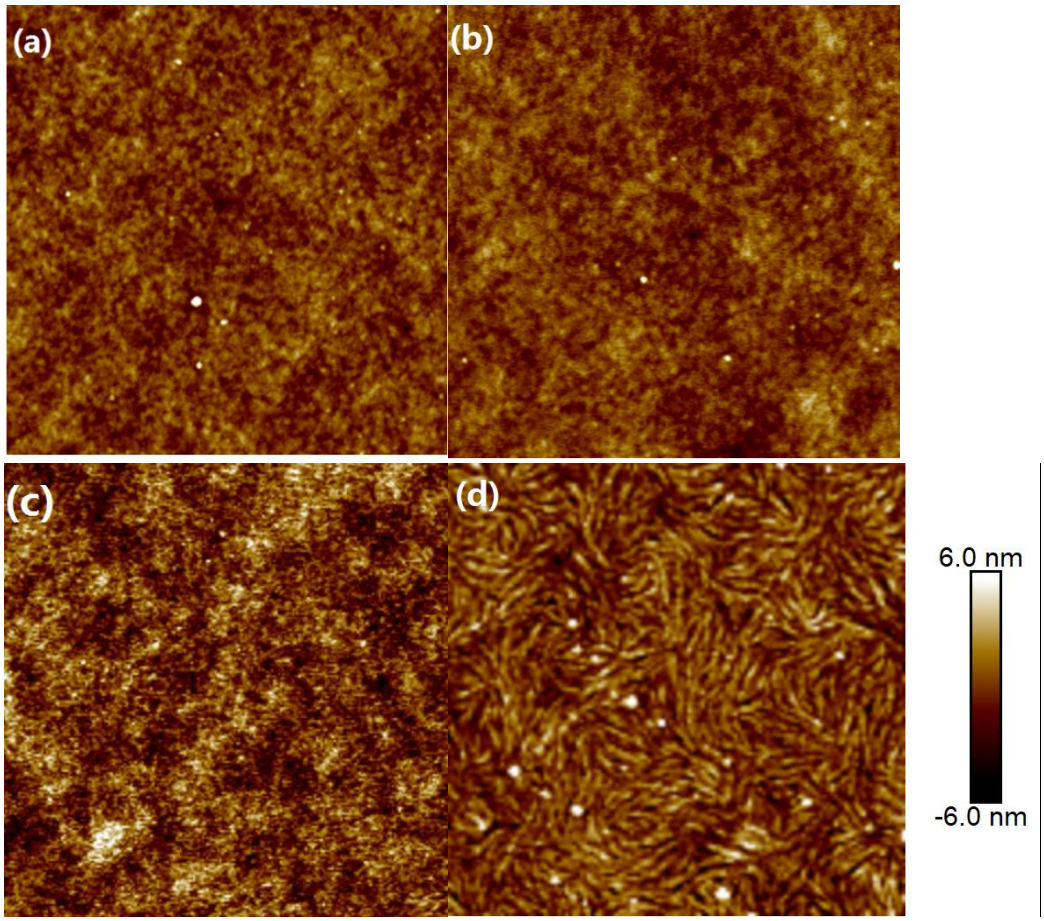

Fig. S16 AFM (3×3 μm) images of (a) ITO/ PEDOT:PSS/ PTQ10:IDIC-2F, (b) ITO/ PEDOT:PSS-GO/ PTQ10:IDIC-2F, (c) ITO/ PEDOT:PSS/ PTQ10:IDIC-2F/PDINO, (d) ITO/ PEDOT:PSS/ PTQ10:IDIC-2F/PDINO-G

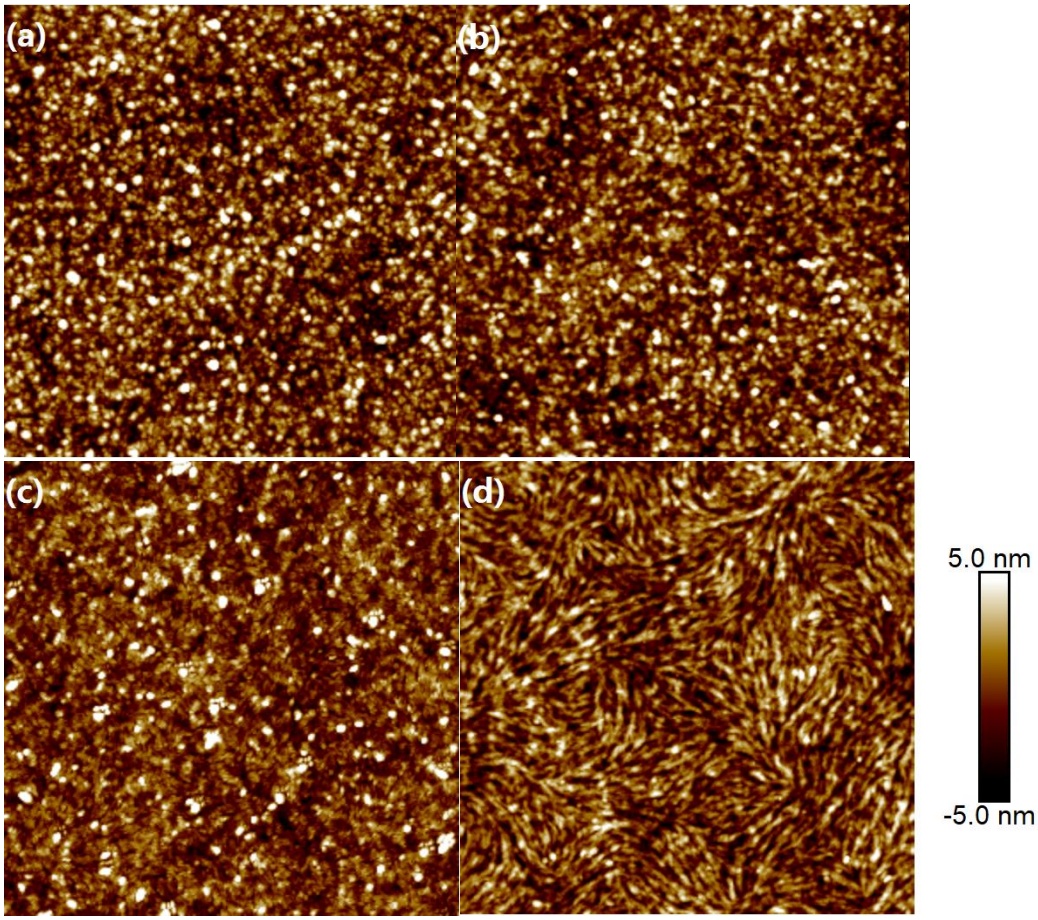

Fig. S17 AFM (3×3 μm) images of (a) ITO/ PEDOT:PSS/ PTQ10:IDIC, (b) ITO/ PEDOT:PSS-GO/ PTQ10:IDIC, (c) ITO/ PEDOT:PSS/ PTQ10:IDIC/PDINO, (d) ITO/ PEDOT:PSS/ PTQ10:IDIC/ PDINO-G

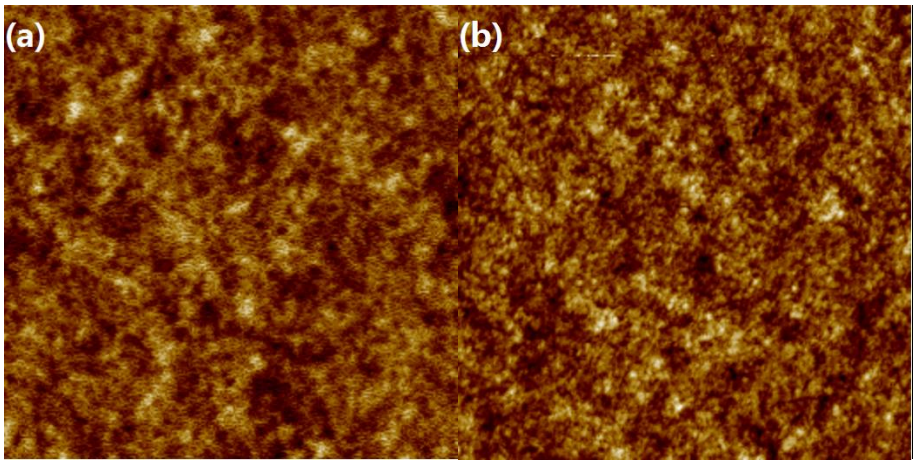

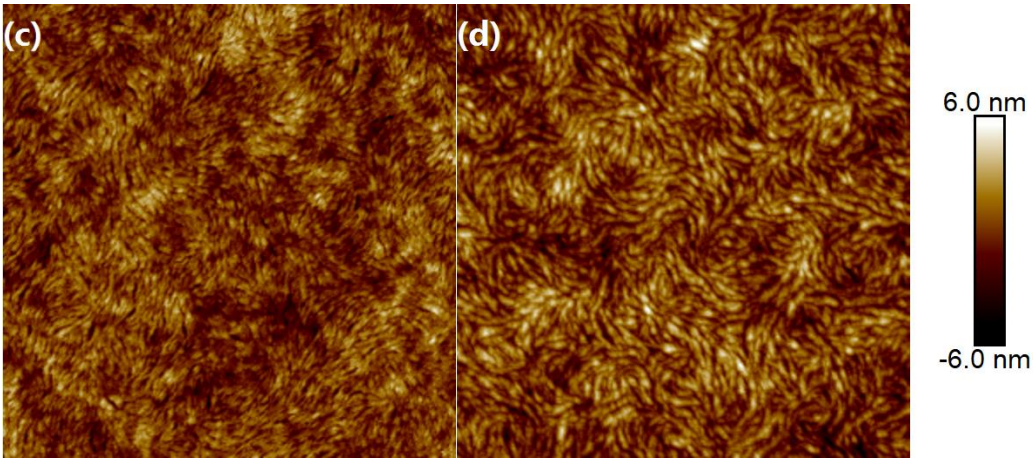

Fig. S18 AFM (3×3 μm) images of (a) ITO/ PEDOT:PSS/ PM6:Y6, (b) ITO/ PEDOT:PSS-GO/ PM6:Y6, (c) ITO/ PEDOT:PSS/ PM6:Y6/ PDINO, (d) ITO/ PEDOT:PSS/ PM6:Y6/ PDINO-G

Table S14 The roughness analysis of conducting atomic microscopy (AFM) results.

Blend Films	Structure of OSCs with different interfacial modification	RMS (nm)
PTQ10:IDIC-2F	ITO/PEDOT: PSS/BHJ	0.96
	ITO/PEDOT: PSS-GO/BHJ	0.98
	ITO/PEDOT: PSS/ BHJ/PDINO	0.91
	ITO/PEDOT: PSS/ BHJ/PDINO-G	1.49
PTQ10:IDIC	ITO/PEDOT: PSS/BHJ	2.41
	ITO/PEDOT: PSS-GO/BHJ	2.29
	ITO/PEDOT: PSS/ BHJ/PDINO	2.17
	ITO/PEDOT: PSS/ BHJ/PDINO-G	1.68
PM6:Y6	ITO/PEDOT: PSS/BHJ	1.28
	ITO/PEDOT: PSS-GO/BHJ	1.33
	ITO/PEDOT: PSS/ BHJ/PDINO	1.24
	ITO/PEDOT: PSS/ BHJ/PDINO-G	1.35

16. Stability

In order to evaluate the stability of the OSCs based on PTQ10: IDIC-2F with graphene containing interlayer, we measure the photostability and shelf-stability of inverted devices with simple encapsulation by water- and oxygen-barrier films. The variation tendency of shelf-stability parameters is shown in Fig. S19a. We find stable V_{OC}, while the J_{SC} and *FF* degrade slightly (<5%), and the PCE of the inverted structured OSCs remained 94.23% of their initial value after around 250 h of storage under N_2 atmosphere. The photostability was measured under continuous 1 sun illumination at max power point in the glove box filled with nitrogen. The evolution of photostability parameters are shown in Fig. S19b. The PCE remains approximately 65.12% after about 250 h continuous illumination. The decrease of efficiency could be due to the chemical structure degradation of the double bonds in the small molecule acceptor under the continuous illumination.

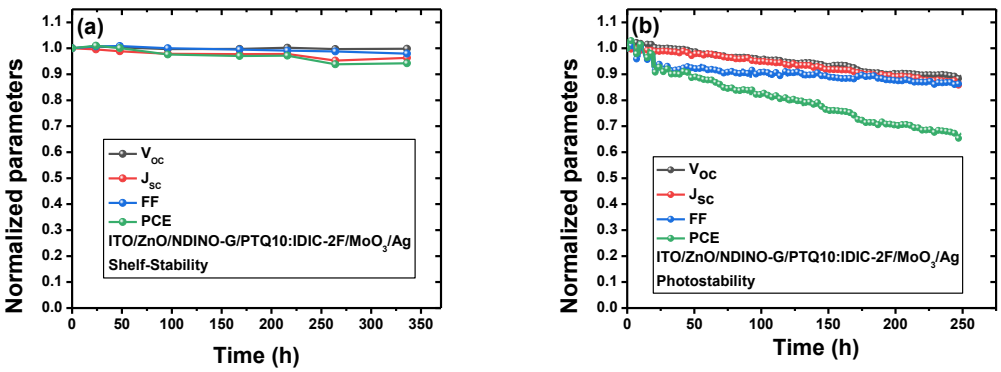

Fig. S19 Shelf-stability (a) and photostability (b) for inverted devices based on PTQ10: IDIC-2F with NDINO-G, the photostability measured under continuous 1 sun illumination at max power point in the glove box filled with nitrogen.

17. The Test Report of NIM

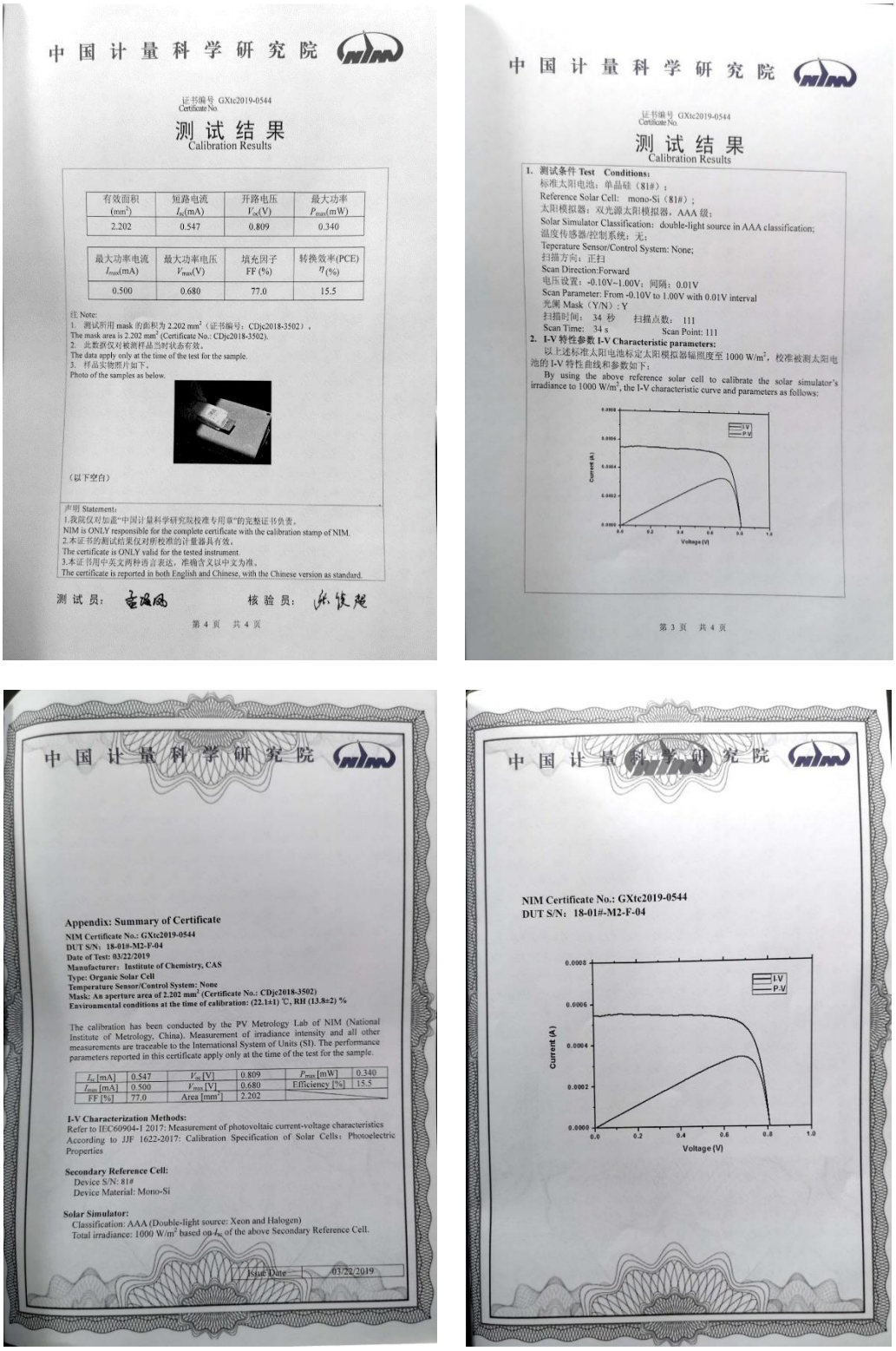

中国计量科学研究院

证书编号 GXtc2019-0544
Certificate No.

测试结果
Calibration Results

有效面积 (mm^2)	短路电流 I_{sc}(mA)	开路电压 V_{oc}(V)	最大功率 P_{max}(mW)
2.202	0.547	0.809	0.340

最大功率电流 I_{max}(mA)	最大功率电压 V_{max}(V)	填充因子 FF (%)	转换效率(PCE) η (%)
0.500	0.680	77.0	15.5

注 Note:
1. 测试所用 mask 的面积为 2.202 mm^2（证书编号：CDjc2018-3502），
The mask area is 2.202 mm^2 (Certificate No.: CDjc2018-3502).
2. 此数据仅对被测样品当时状态有效。
The data apply only at the time of the test for the sample.
3. 样品实物照片如下。
Photo of the samples as below.

（以下空白）

声明 Statement：
1.我院仅对加盖"中国计量科学研究院校准专用章"的完整证书负责。
NIM is ONLY responsible for the complete certificate with the calibration stamp of NIM.
2.本证书的测试结果仅对所校准的计量器具有效。
The certificate is ONLY valid for the tested instrument.
3.本证书用中英文两种语言表述，准确含义以中文为准。
The certificate is reported in both English and Chinese, with the Chinese version as standard.

测试员： 核验员：

第 4 页 共 4 页

中国计量科学研究院

证书编号 GXtc2019-0544
Certificate No.

测试结果
Calibration Results

1. 测试条件 Test Conditions:
标准太阳电池：单晶硅（81#）；
Reference Solar Cell: mono-Si（81#）;
太阳模拟器：双光源太阳模拟器，AAA 级；
Solar Simulator Classification: double-light source in AAA classification;
温度传感器/控制系统：无；
Teperature Sensor/Control System: None;
扫描方向：正扫
Scan Direction:Forward
电压设置：-0.10V~1.00V；间隔：0.01V
Scan Parameter: From -0.10V to 1.00V with 0.01V interval
光阑 Mask（Y/N）: Y
扫描时间：34 秒 扫描点数：111
Scan Time: 34 s Scan Point: 111
2. I-V 特性参数 I-V Characteristic parameters:
以上述标准太阳电池标定太阳模拟器辐照度至 1000 W/m^2，校准被测太阳电池的 I-V 特性曲线和参数如下：
By using the above reference solar cell to calibrate the solar simulator's irradiance to 1000 W/m^2, the I-V characteristic curve and parameters as follows:

第 3 页 共 4 页

中国计量科学研究院

Appendix: Summary of Certificate
NIM Certificate No.: GXtc2019-0544
DUT S/N: 18-01#-M2-F-04
Date of Test: 03/22/2019
Manufacturer: Institute of Chemistry, CAS
Type: Organic Solar Cell
Temperature Sensor/Control System: None
Mask: An aperture area of 2.202 mm^2 (Certificate No.: CDjc2018-3502)
Environmental conditions at the time of calibration: (22.1±1) ℃, RH (13.8±2) %

The calibration has been conducted by the PV Metrology Lab of NIM (National Institute of Metrology, China). Measurement of irradiance intensity and all other measurements are traceable to the International System of Units (SI). The performance parameters reported in this certificate apply only at the time of the test for the sample.

I_{sc} [mA]	0.547	V_{oc} [V]	0.809	P_{max} [mW]	0.340
I_{max} [mA]	0.500	V_{max} [V]	0.680	Efficiency [%]	15.5
FF [%]	77.0	Area [mm^2]	2.202		

I-V Characterization Methods:
Refer to IEC60904-1 2017: Measurement of photovoltaic current-voltage characteristics
According to JJF 1622-2017: Calibration Specification of Solar Cells: Photoelectric Properties

Secondary Reference Cell:
Device S/N: 81#
Device Material: Mono-Si

Solar Simulator:
Classification: AAA (Double-light source: Xeon and Halogen)
Total irradiance: 1000 W/m^2 based on I_{sc} of the above Secondary Reference Cell.

Issue Date	03/22/2019

中国计量科学研究院

NIM Certificate No.: GXtc2019-0544
DUT S/N: 18-01#-M2-F-04

Fig. S20 The certificate of inverted OSCs devices by the National Institute of Metrology, China.

Reference

1 J. Junquera, O. Paz, D. Sanchez-Portal and E. Artacho, *Phys. Rev. B: Condens. Matter Mater. Phys.*, 2001, 64, 235111.

2 N. Troullier, J. L. Martins, *Matter Mater. Phys.*, 1991, 43, 1993.

3 L. Zhang, Z. J. Zhang, C. Z. He, L. M. Dai, J. Liu an L. X. Wang, *ACS Nano*, 2014, 8, 6663–6670.

4 P. W. M. Blom and M. C. J. M. Vissenberg, *Mater. Sci. Eng.*, 2000, 27, 53.

5 K. Zhao, L. Ye, W. Zhao, S. Zhang, H. Yao, B. Xu, M. Sun, J. Hou, *J. Mater. Chem. C*, 2015, 3, 9565.